

X-ray source design optimization using differential evolution algorithms—A case study

Cite as: Rev. Sci. Instrum. 93, 053101 (2022); doi: 10.1063/5.0079389

Submitted: 20 November 2021 • Accepted: 30 March 2022 •

Published Online: 3 May 2022



View Online



Export Citation



CrossMark

Weizhong Yan, Ye Bai, Rui Xu, and V. Bogdan Neculaes^{a)}

AFFILIATIONS

GE Research, Niskayuna, New York 12309, USA

^{a)}Author to whom correspondence should be addressed: neculaes@research.ge.com

ABSTRACT

Traditional x-ray sources used today for multiple applications, such as medical imaging (computed tomography, radiography, mammography, and interventional radiology) or industrial inspection, are vacuum based electron beam devices that include several key components, such as electron emitters, electron guns/cathodes, and anodes/targets. The associated electronics for electron beam generation, focusing and control, and beam acceleration are located outside the vacuum chamber. The general topology of these tubes has been directionally unchanged for more than 100 years; however, tube design remains a long, inefficient, tedious, and complex process; blind design of experiments do not necessarily make the process more efficient. As a case study, in this paper, we introduce the differential evolution (DE), an artificial intelligence-based optimization algorithm, for the design optimization of x-ray source beam optics. Using a small-scale design problem, we demonstrate that DE can be an effective optimization method for x-ray source beam optics design.

Published under an exclusive license by AIP Publishing. <https://doi.org/10.1063/5.0079389>

I. INTRODUCTION AND MOTIVATION

For more than 100 years, x-ray sensing has become ubiquitous in multiple applications, such as medical imaging, industrial nondestructive evaluation, security, and analytical imaging. After the introduction of the modern, industrialized x-ray tube by GE in 1913, the Coolidge x-ray tube, the impact of this device,¹ and the associated imaging techniques have been growing dramatically. For example, in the medical imaging space, x-ray sources enable 3D Computed Tomography (CT), interventional radiology, mammography, traditional radiography (chest, abdomen, etc.), bone densitometry, dental imaging, and so on. Only in the USA, more than 70×10^6 CT imaging exams are performed every year.²

The basic principles of generating x rays in commercially available x-ray sources/tubes have remained the same for over a century: an electron emitter, typically a thermionic emitter (heated tungsten), generates a beam that is focused and accelerated toward an anode/target; the acceleration voltage ranges from tens of kV (for mammography) to more than 100 kV (for CT) but can reach hundreds of kV in x-ray sources used in industrial nondestructive evaluation. The accelerated electron beam interacts with the anode/target and while more than 99% of the beam energy translates into heat at the anode, a small fraction (<1%)¹ is converted

into x rays via Bremsstrahlung processes. The x-ray photons are leveraged downstream for imaging. These x-ray sources are vacuum tubes, most of which are sealed and have a pressure on the order of 10^{-6} Torr. Lower power x-ray sources tend to have stationary anodes/targets, whereas higher power x-ray sources use a rotating anode/target to prevent melting upon the interaction with the electron beam (the beam always hits a “fresh” area of the rotating anode). While new technological innovations have been tested in the last 40–50 years, for example, replacing thermionic electron emitters with cold electron emitters like Carbon Nano Tubes (CNT) or Spindt emitters³ or replacing ball bearings for anode rotation with liquid metal bearings,¹ the overall x-ray source topology and physics principles have remained the same for more than a century.

The design and optimization of x-ray sources is a complex, multidisciplinary process involving material science, vacuum physics, electromagnetics, mechanical engineering, thermal management science, etc. For example, a customized electron gun and beam focusing elements need to be designed so that the electron beam size when it interacts with the anode meets the requirements of the specific imaging application—the size of the electron beam hitting the anode, termed “focal spot,” critically impacts the spatial resolution of the image generated by the imaging system using this x-ray source. High spatial resolution enabled by the smaller size

of the electron beam allows the radiologist to distinguish small anatomical features of interest (tumors, for example). Therefore, x-ray sources need not only to generate enough Bremsstrahlung photons for imaging (via higher beam currents) but the beam needs also be focused to a smaller size to enable high spatial resolution for imaging. Since it is more challenging to focus higher current electron beams to smaller sizes due to space charge effects, an x-ray source design goal needs not only to identify the optimum value of the beam current and the beam optics solution that enables enough production of x-ray photons but also to maintain a small enough spot size that can be accomplished with a practical beam optics solution. Essentially, x-ray source design involves choosing an optimum parameter combination by exploring a parameter space with tens (or even higher numbers) of parameters—a process that has been largely driven by human intuition for the last 100 years. X-ray source design is a long, inefficient, tedious, and complex process; blind DOEs (design of experiments) do not necessarily make the process much more efficient. The advent of intelligent design driven by the increased computational power of modern computers as well as by the introduction of powerful optimization algorithms has the potential to revolutionize x-ray source design and optimization. This paper shows a case study using artificial intelligence (AI) techniques for x-ray source design and optimization.

For more than a decade now, AI techniques have been successfully applied to various charged particle beam applications for design and optimization as well as control of these devices in operation. For example, genetic algorithms (GA),⁴ differential evolution (DE) algorithms,⁵ and machine learning with surrogate modeling⁶ have been adopted for particle accelerators design exploration.

Beyond large scale particle accelerators, the vacuum electronics community tested intelligent designs for a variety of devices, including traveling wave tubes (TWTs),⁷ compact MeV range electron beam accelerators,⁸ klystrons,⁹ and magnetrons.¹⁰

To the best of our knowledge, AI techniques have not been actively used for x-ray tube design. This work presented here is a case study to show the feasibility of leveraging optimization algorithms for x-ray source design optimization. Like other design optimization problems, the key challenge we address here is to minimize the number of human evaluations or simulations, each of which is a process involving a human in the loop as well as expensive computing time. To address this challenge, we used the differential evolution (DE) algorithm, an AI-based optimization technique, for the design optimization of x-ray source beam optics. DE is a population-based, metaheuristic optimization method. Compared to other metaheuristic optimization methods, DE is simple to use and has generally good performance for various optimization problems.¹¹ DE has also been adopted for engineering design optimization problems.^{12–16} However, using DE for the design optimization of x-ray source beam optics has never been done. Through the case study, in this paper, we have demonstrated that by using DE, we can achieve the optimal design in only five generations, a total of 107 simulations/evaluations.

The rest of this paper is organized as follows. Section II discusses x-ray source beam optics design, the problem of interest in this paper. General discussions of differential evolution algorithms are given in Sec. III. Section IV provides details of using DE for x-ray source beam optics design optimization, and Sec. V concludes this paper.

II. X-RAY SOURCE BEAM OPTICS DESIGN

A. X-ray source beam optics design model

Typical beam optics for x-ray sources involves the design of the electron emitter, the electron gun, electromagnetic focusing lenses, and cathode-anode spacing and topology so that a beam current accelerated at a certain voltage between the anode and the cathode is focused to a specific spot size: essentially, a Maxwell equation driven electromagnetics problem. These elements include the design optimization of various components, such as mechanical dimensions, position on the beam line, materials (conductors and insulators), mechanical tolerances, and identifying potential voltage biases for the focusing elements. If beam focusing is performed electrostatically, this means designing various metallic structures to be biased at specific voltages that serve the function of focusing the beam. If the focusing system has a combination of electrostatic and electromagnetic lenses, these electromagnetic lenses for beam focusing and/or beam deflection need to be also designed, including the specific lens topology (dipole, quadrupole, solenoid, etc.), materials in the lens (wire size and material, number of windings, and support structures), physical dimensions, and specific powering up parameters (what magnetic fields need to be generated by these lenses and what electric current is needed to power up the lenses in order to generate the desired magnetic field), and so on. While some x-ray sources may have a specific beam current (mA) accelerated by a specific anode-cathode voltage (kV) that needs to be focused to a specific spot size (length and width of the spot size), most x-ray sources need to accommodate multiple focusing points of interest as well as multiple combinations of them (mA, kV, and length and width of the spot size). This increases dramatically the complexity of the design process. All of these must take into account a number of constraints: the life of the electron emitter must be reasonable (a trade-off between the size of the electron emitter and the beam current needed to be generated by this emitter), the beam optics design must have realistic mechanical tolerances for a practical product, electrical signals also must have realistic metrics (finite precision of the electrical circuits), and the anode/target cannot be melted by concentrating the electron beam to a very small spot size.

While for real x-ray tubes, the size of the electron beam/beam optics depends on tens of variables; for the test case here, we considered the optimization space of three variables: two geometrical variables (distances) and one electrical variable (bias voltage). The three variables (see definitions in Fig. 1) are negative bias voltage X1, set the height of cathode emitter X2, and the shortest gap between the anode and the vacuum vessel X3. In this model, a 6 mm long cylindrical emitter has been selected as the thermionic (tungsten) electron emitter. The diameter of the emitter is set to 0.9 mm. The temperature of the emitter is set to 2750 K.

B. Three-dimensional beam optics simulator

Opera 3D is the pre-processing and post-processing commercial software for electromagnetics, thermal, and mechanical stress solutions. Finite element discretization forms the basis of the methods used in these analysis programs. This widely applicable technique for the solution of partial differential equations requires special enhancements to make it applicable to more accurate electromagnetic field calculations.¹⁷

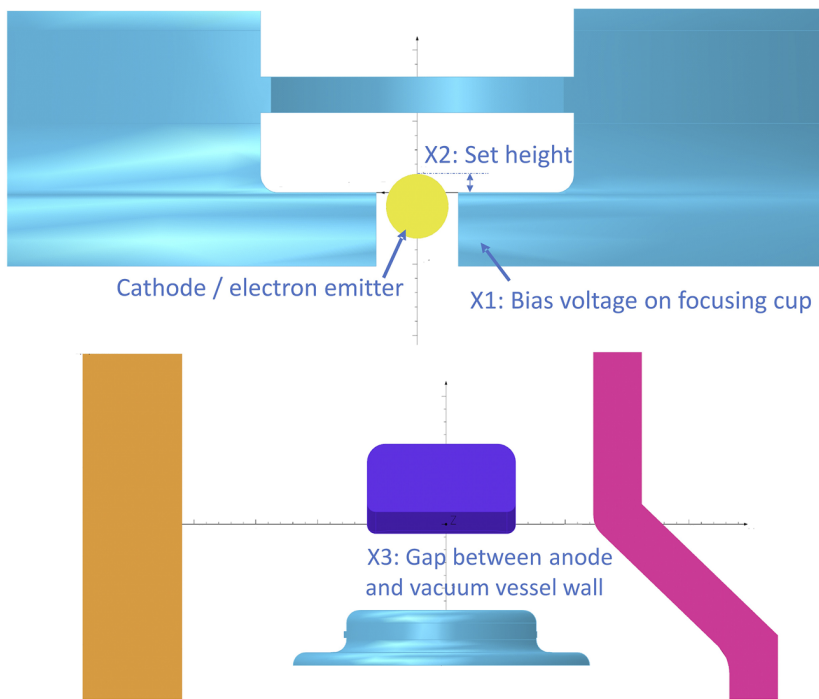


FIG. 1. Variables X1, X2, and X3 used to control beam optics and spot size for our test case.

The Geometric Modeler and Pre-Processor provide access to these features. These programs provide facilities for the creation of finite element models, the specification of complex conductor geometry, the definition of material characteristics (including non-linear, anisotropic, and hysteretic materials), and the interaction of graphical displays with an examination of the data.

Similarly, the Post-Processor provides facilities necessary for calculating electromagnetic, temperature, and displacement fields

and displaying them as graphs and contour maps. The Post-Processor can calculate and display many derived quantities and also plot particle trajectories through electromagnetic fields.

Different solvers or modules have been used to solve different physics problems in Opera. The Charged Particle solver can be used to compute electrostatic fields in three dimensions, including the effects caused by space charge in beams of charged particles. Secondary particles produced as a result of collisions, as well as the

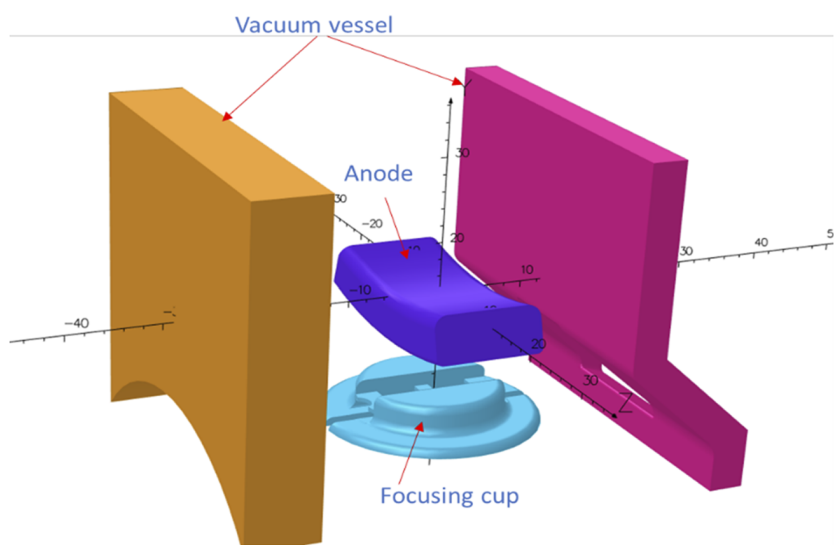


FIG. 2. Opera-3D model used for beam optics simulation. For simplicity and clarity, only sections of the vacuum chamber and the anode/target are shown.

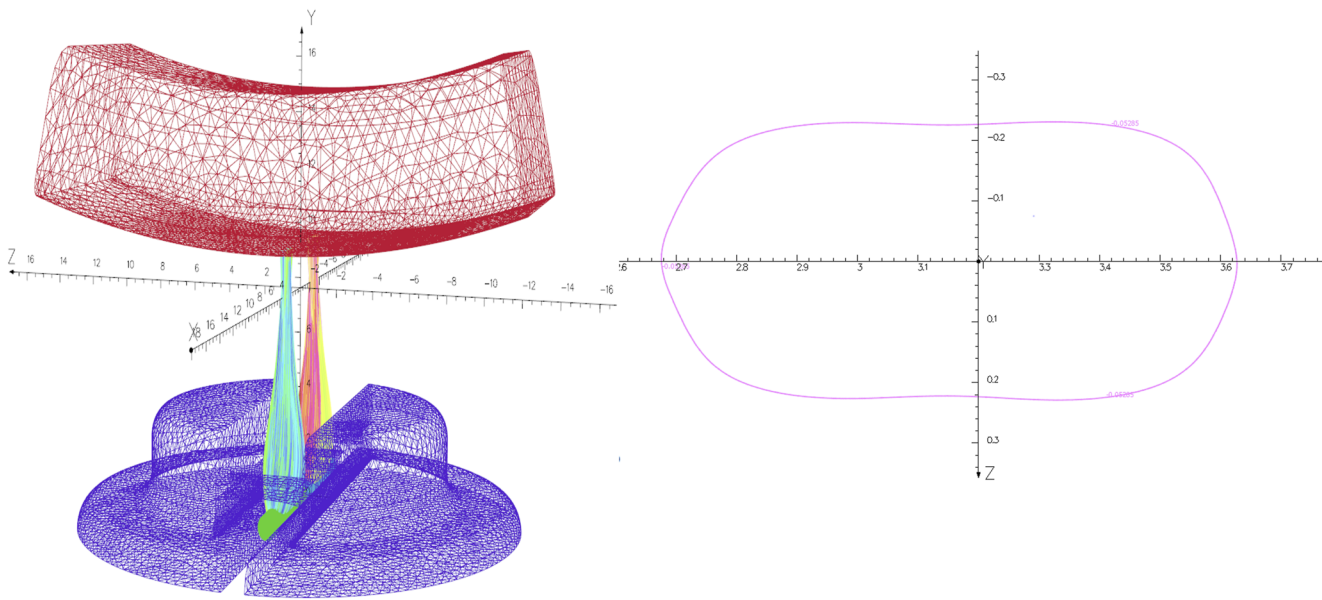


FIG. 3. Simulation results of beam trajectories (left hand side) and focal spots (right hand side).

effects of the magnetic fields created by the charged particle beam, can be included in the calculation. The program incorporates state of the art algorithms for the calculation of electromagnetic fields, advanced finite elements, and nonlinear equation numerical analysis procedures.¹⁸

The Charged Particle solver uses the finite element method to solve the electrostatic Poisson's equation and calculate the electric scalar potential in the following equation:

$$\nabla \cdot \epsilon \nabla V = -\rho, \quad (1)$$

where V is the electrostatic potential, ϵ is the dielectric permittivity tensor, and ρ is the charge density. In the Charged Particle solver used in this paper, different types of particle emission models can be used to create the primary beams of charged particles. These include thermal emission models, field effect emission models, plasma emission models, and user defined emission models.

In this paper, Child's law (2) and Langmuir/Fry relationships have been used for the calculation of the space charge limited current j_e from a thermionic emitter in the model,¹⁹

$$j_e = \frac{4\epsilon_0}{9} \sqrt{\frac{2q}{m_0}} \frac{V_0^{3/2}}{d^2}, \quad (2)$$

where ϵ_0 is the permittivity of free space, q is the charge on the particle, m_0 is the particle rest mass, and V_0 is the accelerating voltage applied to the accelerating gap d .

Figure 2 shows the 3D model used for beam optics simulations, which include the electron emitter, focusing cup/electron gun, anode/target, and the vacuum vessel. A constant of -30 kV voltage has been applied on the cathode emitter, whereas the voltage on the anode and the vacuum vessel is set to 0 V (ground potential);

essentially, the electron beam is accelerated to 30 kV before interacting with the anode/target. The model in Fig. 3 is a research test variation for a generic x-ray source platform from GE Healthcare. For this simulation study, the electron emitter was considered to be a cylinder made of tungsten (thermionic electron emitter); this is a simplification of real x-ray tubes, where most often the electron emitter is either a coil/filament or a flat W emitter.

To balance 3D FEM calculation time and simulation accuracy, the mesh size of key components has been selected carefully. A mesh size of 0.1 mm has been used on electron emitters and focusing cup/electron guns where precise electrostatic field distribution will be critical for accurate electron beam simulation results. Larger mesh sizes from 0.5 to 2 mm have been selected for the anode and the vacuum vessel that are far away from the emitter to shorten the total simulation time.

Figure 3 shows the simulation results of electron beam trajectories and focal spots on the surface of the anode. The simulation outputs are focal spot width Y_1 and length Y_2 , which are measured at 15% of the maximum intensity.

The initial population of the three input variables X_1 , X_2 , and X_3 (see Fig. 1) has been generated via random samplings from the range of the parameter presented in Table I (as discussed in

TABLE I. Design variables and their ranges.

Design variables (Xs)	Initial value	Upper range limit	Lower range limit
X1: V_bias (V)	-40	-20	-80
X2: Set height (mm)	0.30	0.15	0.35
X3: Frame wall distance (mm)	5	8	3

Sec. IV of this paper). The subsequent generations of solutions were generated using the Matlab DE algorithm. Thus, five generations of solutions will create at least 107 Opera-3D models (see details in Sec. IV), which takes significant computation time. Special scripts have been used to generate those models and run data post-processing automatically.

III. DIFFERENTIAL EVOLUTION ALGORITHMS

Differential evolution (DE) is a population-based, metaheuristic optimization method that is a part of the family of evolutionary algorithms (EA). Introduced by Storn and Price in the 1990s, DE performs optimization by iteratively improving the candidate solutions (populations) via its specially designed vector differences-based perturbation mechanism.²⁰ Because of its original design, DE works particularly well for optimization problems with real valued (continuous) design space (parameters). Similar to its peer methods in the EA family, such as GA (genetic algorithms), DE is a derivative-free method, that is it does not need the optimization function to be continuous and differentiable. In addition, like other EA methods, DE is a stochastic global optimization method that is capable of handling large design spaces and complex fitness landscapes. It is worth pointing out that metaheuristic optimization methods, including DE, do not ensure that an optimal solution will ever be found.

One key distinct characteristic/principle of DE is that its search step is inherently adaptive during the evolutionary process.²¹ Such inherent adaptation enables DE to maintain a good trade-off between exploitation and exploration. Another important component of DE that differs from other EA methods is its selection process. DE randomly selects parents from the current population without evaluating their fitness values and uses a greedy selection process, simply picking the better one of the new solution and its parent.²² These distinct characteristics enable DE to outperform generic algorithms (GAs) in numerous optimization applications, as demonstrated in several studies, including Price *et al.*²³

More broadly, compared to other EA methods, DE has several advantages:¹¹ (1) simple and straightforward to use; (2) good performance in terms of accuracy, convergence speed, and robustness for various optimization applications/problems; (3) a relatively small number of design parameters; (4) easily adaptable for integer and discrete optimization; and (5) able to handle large-scale and expensive optimization problems.

Due to the above-mentioned advantages, DE has been successfully used for a wide range of optimization applications, including power plant control,²⁴ decision support,²¹ structural optimization,²⁵ chemical process design,²⁶ and signal processing.¹² DE has also been adopted for engineering design optimization problems, for example, general applications,¹³ turbofan engine cycle parameter designs,¹⁴ turbomachinery airfoil designs,¹⁵ microplasma actuator designs,¹⁶ and water distribution network designs.²⁷ However, to the best of our knowledge, DE has never been used for x-ray tube design optimization.

Differential evolution performs optimization by following the general procedure of evolutionary algorithms (EA). To put it another way, an initial population is first generated by randomly sampling the design space. The fitness of the initial population is then evaluated. The algorithm then enters a loop of successively

improving the population by applying evolution operators, such as mutation, crossover, and selection. Figure 4 illustrates the general procedure of typical DE.

A. Mutation

One key characteristic that makes DE differ from other EAs is its reproduction operator—differential mutation. There are several variants of the DE differential mutation operator.^{11,28} In this paper, we adopt the following differential mutation operator proposed in Ref. 21. Assume the problem has a D -dimensional design space and the population size, i.e., the number of populations per generation is Np . Then, the population for a generation is designated by $\{p_i \in \mathcal{R}^D, i = 1, 2, \dots, Np\}$. For each individual, p_i , in the current generation, the mutation vector, v_i , generated by the differential mutation operator is given in the following:

$$v_i = \beta \cdot p_{bst} + (1 - \beta) \cdot p_i + F \cdot \sum_{k=1}^K (p_{i,k}^a - p_{i,k}^b),$$

where p_{bst} is the best individual in the current population; $p_{i,k}^a$ and $p_{i,k}^b$ are randomly selected, mutually distinct individuals (perturbation vectors) from the current population; K is the number of perturbation vectors; β is a weighting factor representing the greediness of search; and F is the mutation factor representing the level of perturbation.

B. Crossover

All individuals (vectors) in the current generation and the mutated vectors are mixed together via the crossover operator to produce the trial vectors. For j th element of the i th trial vector $u_{i,j}$ is given by

$$u_{i,j} = \begin{cases} v_{i,j} & \text{if } \text{rand}(0, 1) \leq CR \text{ or } j = j_{rand}, \\ p_{i,j} & \text{otherwise,} \end{cases}$$

where the subscript j in all vectors above is j th element of the vector; $\text{rand}(0, 1)$ is a uniform random number between 0 and 1 and

General DE procedure

- 1 Generate an initialize population
- 2 Evaluate the initial population
- 3 Repeat the following:
 - 3.a. Mutation
 - 3.b. Crossover
 - 3.c. Evaluation & Selection
- 4 Until the termination criteria are met

FIG. 4. Differential evolution (DE) typical workflow.

is independently generated for each j and each i ; j_{rand} is a random integer randomly chosen from 1, 2, ..., D; and CR is the crossover probability.

C. Selection

With the parent vector p_i and the trail vector u_i being defined above, the selection operator of DE is to select the better one between the two based on the fitness values $f(\cdot)$. Take a minimization problem as an example, the selected vector for the new generation is defined as

$$p_i^{new} = \begin{cases} u_i & \text{if } f(u_i) < f(p_i), \\ p_i & \text{otherwise.} \end{cases}$$

The weighting factor β , the mutation factor F , and the crossover rate CR are the key design parameters of the DE algorithm, which generally control the balance between exploration and exploitation in the search/optimization process. Even though the three parameters are all in the range of [0, 1], for a given optimization problem, properly setting the parameter values problem-dependently is necessary. Population size N_p is another important DE design parameter that affects optimization performance.

In terms of termination criteria of the DE algorithm, the two most popularly used ones are (1) a pre-specifying fixed number of generations and (2) a pre-specified fitness value. Less frequently used termination criteria include (3) a pre-specified change rate of fitness value and (4) a pre-specified threshold for the maximum distance between every vector in the current population and the best population.²⁹

IV. X-RAY SOURCE BEAM OPTICS DESIGN OPTIMIZATION USING DE ALGORITHM

As discussed in Sec. II, for DE optimization of beam optics in an x-ray source of interest here, we have chosen three design variables: negative bias voltage (X1), set the height of the cathode emitter (X2), and the shortest gap between the anode and the vacuum vessel (X3). The goal for the case study here is to use DE to identify X1, X2, and X3 that will generate a focal spot with a length and width of 430 μm .

The beam current (100 mA) and the beam accelerating voltage (30 kV) were maintained constant in simulations. For example, a focal spot of hundreds of micrometers is typically needed in mammography and interventional radiology medical imaging applications. The design space is defined by the lower and upper bounds of the three design variables, as presented in Table I.

Since any practical measurement validation of the electron beam footprint on the anode/focal spot has inherent experimental uncertainty, it is not useful to run optimization studies to meet the desired specifications within several micrometers; a more reasonable goal should be to be within several tens of micrometers of the 430 μm metric. Another key reason for not spending resources to optimize the beam optics design so that the simulated focal spot is within micrometers of the desired goal is that there would be differences between the simulated spot and the experimentally measured spot.

Once a design that meets this goal has been identified, an experimental build and validation would be the most natural step. Subsequent design refinement of the first build would bring the x-ray source topology toward meeting the medical imaging needs of interest; vacuum tube studies involve the build of several iterations, and performance evaluation of these intermediate designs until the final topology is identified. Because of the complex physics of vacuum tubes, a complete, initial computational design using software packages followed by the build of the first iteration that would automatically meet all x-ray source needs is not possible—several generations of hardware are normally needed in the quest to appropriately solve the design problem.

Since the simulation outputs are the width (Y1) and length (Y2) of the focal spot (see Fig. 3), which characterize the electron beam footprint on the anode (the focal spot), we use Y1 and Y2 to define the fitness function (optimization objective) of our optimization. Specifically, our goal here is to optimize the beam optics design so that Y1 and Y2 are as close as possible to 430 μm , which is an example of a metric that is beneficial in medical imaging. That is, the fitness function used to optimize our DE for our case study is

$$y = \max(|y_1 - 430|, |y_2 - 430|).$$

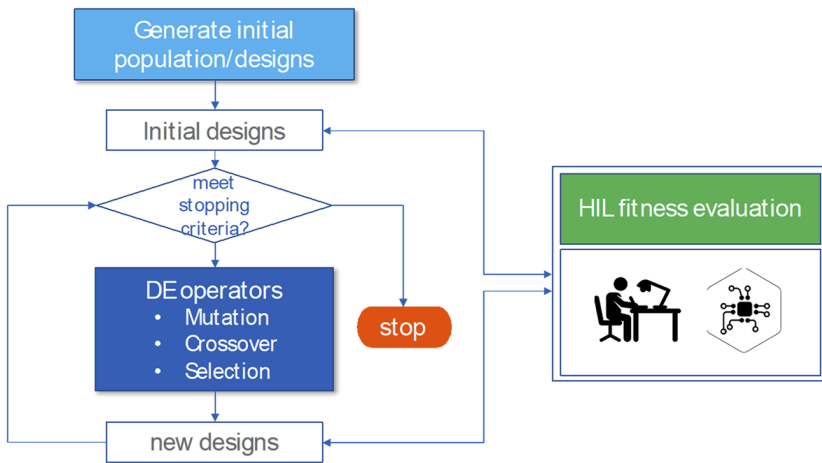


FIG. 5. DE optimization workflow with human-in-the-loop (HIL) fitness evaluation.

Mathematically, our optimization problem is defined as

$$\min_{x_1, x_2, x_3} y, \text{s.t.} \begin{cases} L_1 \leq X_1 \leq U_1, \\ L_2 \leq X_2 \leq U_2, \\ L_3 \leq X_3 \leq U_3, \end{cases}$$

where $L_i, i = 1, 2, 3$ and $U_i, i = 1, 2, 3$ are lower and upper bounds of X_1, X_2 , and X_3 , respectively.

Figure 5 depicts the high-level workflow of our DE optimization used in this study. As in all other evolutionary algorithms, fitness evaluation is an important component in our DE optimization. One thing that is worth pointing out is that our fitness evaluation is a manual (human-in-the-loop) process that includes 3D model generation, postprocessing, and spot size measurement, all of which are computationally and labor intensive. Minimizing the number of fitness evaluations in the process of DE optimization is the key consideration in our case study.

As discussed in Sec. III, DE optimization has several design parameters. For the x-ray source beam optics optimization studied in this paper, the following DE design parameters were chosen: population size N_p is 20 (with an initial population size of 27); weighting factor β is 0.7; mutation factor F is 0.5; and crossover rate CR is 0.3. Since the fitness evaluation is manual and expensive, optimizing these DE design parameters is practically not allowed; instead, we choose the default (most popularly used) DE parameters. Our previous experience with using DE has shown that those

default parameters generally worked well for most of the real-world optimization problems.

The DE algorithms for x-ray source beam optics optimization were all coded in Matlab; the beam optics simulations for obtaining fitness values were performed in Opera 3D.

The initial populations were generated using a 3-factor, 3-level full factorial design, with the three factors being the three design variables, X_1, X_2 , and X_3 , and the three levels being the min, max, and middle values of each design variable. As a result, the initial population has a total of 27 solutions. **Figure 6** shows the fitness values of the initial 27 solutions as well as the response surface (fitness landscape) rendered using radial-based functions (RBF). For ease of visualization, we show (in **Fig. 6**) three response surfaces with respect to design variables X_1 and X_2 , each of which corresponds to one of the three levels of the design variable, X_3 .

Even though the true response surface with respect to the three design variables for the x-ray source beam optics optimization is unknown, the rendered response surfaces depicted in **Fig. 6** help us gain a general sense (a rough idea) of the fitness landscape for optimization. The rendered response surface also allows us to check if the parameter (X s) ranges are properly specified such that the optimum is within the parameter ranges. If no obvious minimum physics is seen within the initially chosen parameter ranges, these parameter ranges should be enlarged to enable scouting for the minimum.

As previously mentioned, while the initial population of 27 solutions was generated using the full factorial design, the subsequent generations of solutions with a population size of 20 were

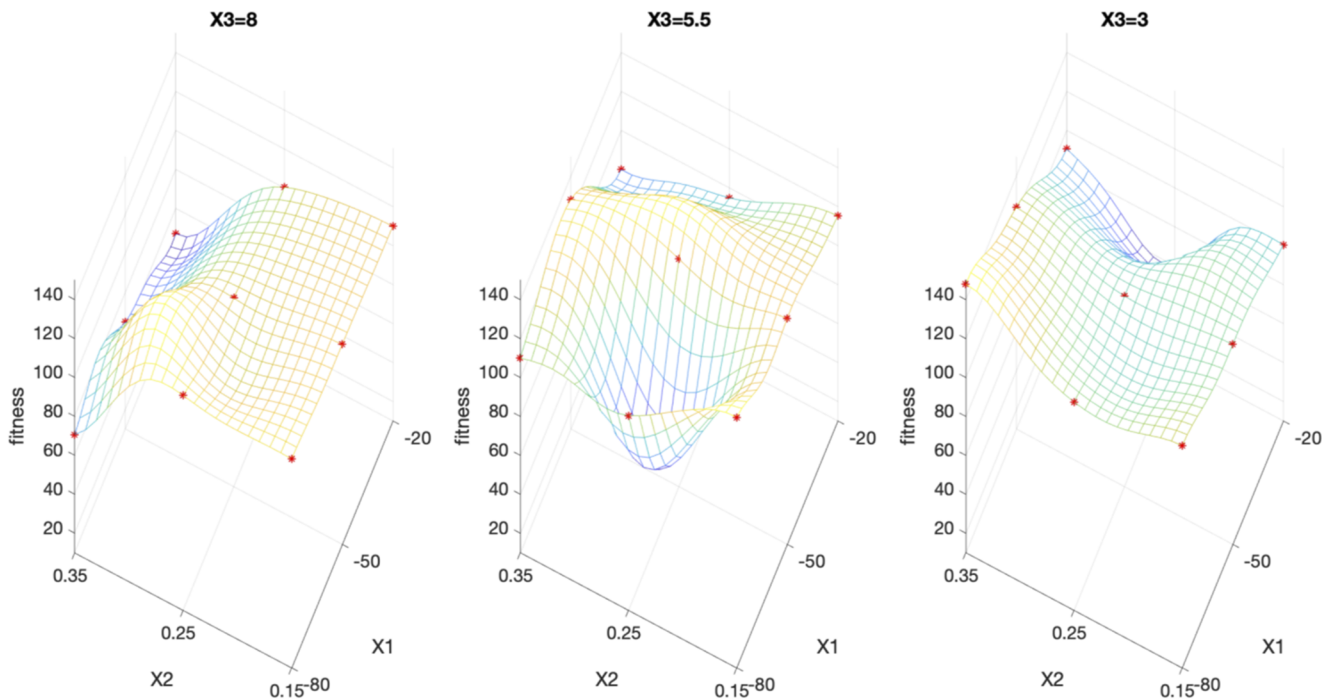


FIG. 6. Rendered response surface based on the 27 designs of the initial population.

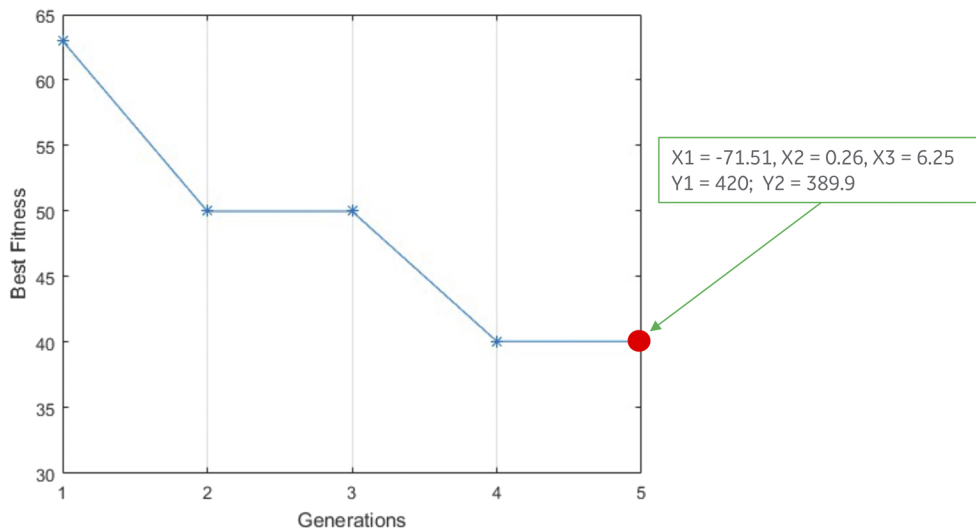


FIG. 7. Fitness values change as the number of generations increases. The optimization stops after five generations.

produced using the Matlab DE algorithm. After 5 generations, a total of 107 ($27 + 4 \times 20$) Opera 3D simulations, the optimization stops. Figure 7 shows the fitness values decrease as the number of generations increases.

The goal for testing the DE approach was to identify X_1 , X_2 , and X_3 so that the beam focal spot has the $430 \times 430 \mu\text{m}^2$ dimensions. Figure 7 shows the X_1 , X_2 , and X_3 values that generate a focal spot with dimensions of $420 \times 390 \mu\text{m}^2$, which is reasonably close to the desired goal. This design would be ready for the initial prototype build and testing; x-ray tube design typically needs several prototype iterations for build and testing. In our experience, an experimentally measured focal spot may be within tens of micrometers of the simulated focal spot; running the DE algorithm for more generations here is not efficient—the results in Fig. 7 are close enough to the desired goal in order to consider an experimental validation.

As an example of generation to generation optimization dynamics, for the first generation of 27 solutions we have observed that: $250 \mu\text{m} < Y_1 < 480 \mu\text{m}$ and $275.2 \mu\text{m} < Y_2 < 389.9 \mu\text{m}$; after the second generation of 20 solutions, we have observed that $300 \mu\text{m} < Y_1 < 480 \mu\text{m}$ and $321.1 \mu\text{m} < Y_2 < 405.2 \mu\text{m}$, narrowing down the search regions for optimizing Y_1 and Y_2 .

V. CONCLUSIONS AND FUTURE WORK

This paper presents a feasibility study using differential evolution (DE) algorithms for the design optimization of beam optics in x-ray tubes. The problem addressed here utilized three input parameters: two physical distances and one bias voltage; the output metrics were the two dimensions of the electron beam footprint on the anode/focal spot. Opera 3D beam optics simulator was utilized to obtain the electron beam focal spot for each design.

The results of this case study demonstrate that DE can be an effective optimization method for x-ray source design and that AI based tools have the potential to re-imagine x-ray source design, more than 100 years after the introduction of the Coolidge x-ray tube topology, which is still leveraged in impactful imaging applications and beyond.

In the future, we may expand this current work toward several research directions. One research direction would be on considering x-ray source design optimization with a larger number of parameters—consider all possible parameters for optimization in Fig. 2. In addition, the fitness function(s) could include not only the size(s) of the electron beam on the anode but also other key success metrics. One of these metrics is the temperature increase of the anode when the impact with the electron beam occurs. X-ray sources want to maximize the electron beam current and minimize the electron beam footprint/focal spot on the anode. They also want to avoid melting or degrading the anode upon interaction with the beam. While, in this study, the beam current (100 mA) and the beam accelerating voltage (30 kV) were kept constant, some classes of medical imaging x-ray sources need specific beam focusing performance for different values of the beam current and the beam acceleration voltage. Expanding this (mA, kV) parameter space to meet practical demand would render a DE algorithm optimization process even more impactful in saving considerable time, compared to the human intuition driven process happening today. For example, x-ray tubes in CT (computed tomography) may need to show similar focal spot metrics/sizes for multiple combinations of beam current and beam acceleration voltage³⁰—DE based design optimization could dramatically shorten the optimization time.

For the conventional DE approach tested here, future research would also involve tuning the DE parameters utilized and exploring larger/smaller sizes for populations of solutions.

Another research direction to be pursued is to tailor the DE algorithmic approach in order to reduce the number of expensive Opera 3D simulations needed to test the fitness function. While considerable effort has been invested in testing genetic algorithms for charged particle beam applications,^{4,7} our test case, the first x-ray tube design optimization exercise, utilized conventional differential evolution algorithms. It would be of interest to consider other types of algorithms for this type of problem, such as particle swarm optimization.

It should be noted that previous researchers often mentioned the use of GA (genetic algorithms) for electron gun type studies;^{31–34}

however, our work explores a new electron gun-based application, x-ray source beam optics optimization, and focuses on using DE (not GA) for the reason presented in Sec. III.

Finally, the method described here may be used for other complex electron beam systems where focal spot size is key, such as electron beam machines for additive manufacturing. The size of the beam, focal spot, determines the resolution of the build in these machines and also impacts the meltpool physics.

ACKNOWLEDGMENTS

The authors thank Pierre Habig (GE Healthcare) for providing guidance on generating the x-ray source test topology and also thank Scott Price (GE Research) for guidance on running the Opera 3D simulations. This work was supported by GE internal.

AUTHOR DECLARATIONS

Conflict of Interest

The authors have no conflicts to disclose.

DATA AVAILABILITY

The data that support the findings of this study are available from the corresponding author upon reasonable request.

REFERENCES

- ¹R. Behling, *Modern Diagnostic X-Ray Sources: Technology, Manufacturing, Reliability* (CRC Press; Taylor & Francis, 2016).
- ²D. J. Brenner, “Slowing the increase in the population dose resulting from CT scans,” *Radiat. Res.* **174**(6b), 809–815 (2010).
- ³V. B. Neculaes, P. Edic, M. Frontera, A. Caiafa, G. Wang, and B. De Man, “Multisource X-ray and CT: Lessons learned and future outlook,” *IEEE Access* **2**, 1568 (2014).
- ⁴A. Hofler, B. Terzic, M. Kramer, A. Zvezdin, V. Morozov, Y. Roblin, F. Lin, and C. Jarvis, “Innovative applications of genetic algorithms to problems in accelerator physics,” *Phys. Rev. Spec. Top.-Accel. Beams* **16**, 010101 (2013).
- ⁵J. Qiang, “Fast longitudinal beam dynamics optimization in x-ray free electron laser linear accelerators,” *Phys. Rev. Accel. Beams* **22**, 094401 (2019).
- ⁶A. Edelen, N. Neveu, M. Frey, Y. Huber, C. Mayes, and A. Adelmann, “Machine learning for orders of magnitude speedup in multiobjective optimization of particle accelerator systems,” *Phys. Rev. Accel. Beams* **23**, 044601 (2020).
- ⁷Y. Hu, Z. Yang, J. Li, B. Li, T. Huang, Q. Hu, X. Jin, X. Zhu, and S. Ma, “Hybrid genetic algorithm for optimization design of traveling wave tubes,” in International Vacuum Electronics Conference, 2008.
- ⁸Z. Tang, “Design of an accelerating tube for a standing-wave accelerator based on genetic algorithm’s optimal calculation,” in 5th International Particle Accelerator Conference IPAC, 2014.
- ⁹H. Pierrick, P. Juliette, M. Claude, and P. Franck, “Klystron efficiency optimization based on a genetic algorithm,” in 2019 International Vacuum Electronics Conference (IVEC), 2019.
- ¹⁰A. Spirkin, P. H. Stoltz, and J. W. Luginsland, “Machine learning investigation of the rising sun magnetron design and operation,” *IEEE Trans. Plasma Sci.* **48**(1), 133 (2020).
- ¹¹S. Das and P. N. Suganthan, “Differential evolution: A survey of the state-of-the-art,” *IEEE Trans. Evol. Comput.* **15**(1), 4–31 (2011).
- ¹²N. Karaboga and B. Cetinkaya, “Design of digital FIR filters using differential evolution algorithm,” *Circuits, Syst. Signal Process.* **25**, 649–660 (2006).
- ¹³T. W. Liao, “Two hybrid differential evolution algorithms for engineering design optimization,” *Appl. Soft Comput.* **10**(4), 1188–1199 (2010).
- ¹⁴X. Zhang, “Optimization on turbofan engine cycle parameter based on improved differential evolution algorithm,” in *2017 17th International Conference on Control, Automation and Systems (ICCAS)* (IEEE, Jeju, 2017), pp. 556–561.
- ¹⁵N. K. Madavan, “Turbomachinery airfoil design optimization using differential evolution,” in *Computational Fluid Dynamics 2002*, edited by S. W. Armfield, P. Morgan, and K. Srinivas (Springer, Berlin, Heidelberg, 2003).
- ¹⁶J. Omidi and K. Mazaheri, “Differential evolution algorithm for performance optimization of the micro plasma actuator as a microelectromechanical system,” *Sci. Rep.* **10**, 18865 (2020).
- ¹⁷Dassault Systems UK Ltd., Opera-3D Reference Manual, Version 19, Kidlington, Oxfordshire UK, 2019.
- ¹⁸C. R. I. Emson, “The computation of electrostatic fields and space charge effects,” in *IEE Colloquium on Computation in Electrostatics*, 26 January 1995.
- ¹⁹A. Khursheed, *The Finite Element Method in Charged Particle Optics* (Kluwer Academic Publishers, Boston, 1999).
- ²⁰R. Storn and K. Price, “Differential evolution—A simple and efficient heuristic for global optimization over continuous spaces,” *J. Global Optim.* **11**(4), 341–359 (1997).
- ²¹F. Xue, A. C. Sanderson, and R. J. Graves, “Multiobjective evolutionary decision support for design-supplier-manufacturing planning,” *IEEE Trans. Syst., Man, Cybern.-Part A* **39**(2), 309–320 (2009).
- ²²M. J. A. Strens and A. W. Moore, “Policy search using paired comparisons,” *J. Mach. Learn. Res.* **3**, 921–950 (2003).
- ²³K. Price, R. M. Storn, and J. A. Lampinen, *Differential Evolution: A Practical Approach to Global Optimization* (Springer-Verlag New York, Inc., 2005).
- ²⁴J. H. Van Sickel, K. Y. Lee, and J. S. Heo, “Differential evolution and its applications to power plant control,” in *Proceedings of the ISAP, International Conference on Intelligent Systems Applications to Power Systems* (IEEE, Niigata, Japan, 2007), pp. 1–6.
- ²⁵M. Georgioudakis and V. Plevris, “A comparative study of differential evolution variants in constrained structural optimization,” *Front. Built Environ.* **6**, 102 (2020).
- ²⁶E. N. Dragoi and S. Curteanu, “The use of differential evolution algorithm for solving chemical engineering problems,” *Rev. Chem. Eng.* **32**(2), 149–180 (2016).
- ²⁷F. Zheng, “Comparing the real-time searching behavior of four differential-evolution variants applied to water-distribution-network design optimization,” *J. Water Resour. Plann. Manage.* **141**(10), 04015016 (2015).
- ²⁸T. Eltaeb and A. Mahmood, “Differential evolution: A survey and analysis,” *Appl. Sci.* **8**(10), 1945 (2018).
- ²⁹K. Zielinski, D. Peters, and R. Laur, “Run time analysis regarding stopping criteria for differential evolution and particle swarm optimization,” in *Proceedings of the 1st International Conference on Experiments/Process/System Modelling/Simulation/Optimization*, 2005.
- ³⁰V. Bogdan Neculaes, Y. Zou, P. Zavodszky, L. Inzenna, X. Zhang, K. Conway, A. Caiafa, K. Frutschy, W. Waters, and B. De Man, “Design and characterization of electron beam focusing for X-ray generation in novel medical imaging architecture,” *Phys. Plasmas* **21**, 056702 (2014).
- ³¹R. Lawrence Ives, Phase II Final Report Computer Optimization of Electron Guns, Calabazas Creek Research, Inc., <https://www.osti.gov/servlets/purl/1011378>.
- ³²C. N. Ribton, “Development of an electron gun design optimization methodology,” Ph.D. dissertation (Brunel University London, 2017).
- ³³C. Ribton, S. del Pozo, W. Balachandran, and D. R. Smith, “Design of electron guns using a bespoke genetic algorithm,” *J. Electrotech. Electron.* **51**(5–6), 120–128 (2016).
- ³⁴Z. Tang, Y. Pei, X. Yang, Y. Yu, and W. Zhang, “Optimal design of a photocathode electron gun with high-brightness and high-repetition rate based on genetic algorithm,” in *Proceedings of the 7th International Particle Accelerator Conference (IPAC 2016)*, Busan, Korea, 8–13 May 2016.